https://doi.org/10.5194/egusphere-2026-1523
Preprint. Discussion started: 10 April 2026

Operational damage misclassification in scenario-based ShakeMaps: evidence from station-updated ground-motion fields in a deep-basin urban environment

Fatma İ. Kara[1]

[1] Department of Architecture, Gebze Technical University, Gebze, Kocaeli, 41400, Türkiye

Correspondence to: Fatma İ. Kara (figokce@gtu.edu.tr)

Abstract. Near-real-time ShakeMap-based damage assessments are widely used to support rapid post-earthquake decision-making. However, their operational reliability depends on how accurately ground-motion fields represent local site and basin effects. This study investigates the potential for operational damage misclassification arising from purely scenario-based ShakeMap representations in deep-basin urban environments.

The 30 October 2020 Samos earthquake was analysed for the Mansuroğlu Neighborhood (Bayraklı District, Izmir, Türkiye) using a two-stage framework: (i) a scenario-based rapid damage estimation and (ii) a station-updated near-real-time configuration incorporating strong-motion recordings from Disaster and Emergency Management Authority of Türkiye (AFAD) stations located within a 3 km radius.

Results show that the scenario-based configuration systematically underestimates intermediate-period spectral demand (T = 0.6–1.0 s), which governs the response of the predominantly mid-rise reinforced concrete building stock. These discrepancies propagate into cumulative damage exceedance probability estimates. While the scenario-based approach largely confines the {Moderate + Extensive + Collapse} exceedance probability to the 0–10 % range, station-based updating increases this range to approximately 15–30 % in critical zones.

This shift represents a transition across an operationally meaningful threshold with direct implications for response categorization and resource prioritization during the early post-earthquake phase. The findings demonstrate that misclassification risk in rapid damage assessment arises not only from modelling uncertainty but also from threshold-sensitive distortions in exceedance estimation.

Even a limited number of spatially proximal strong-motion stations can substantially enhance the robustness of ground-motion representation. The study therefore highlights ShakeMap calibration as a governance-relevant intervention in seismic risk management rather than merely a technical refinement.

1 Introduction

In seismically active regions, rapid post-earthquake damage assessment plays a critical role in supporting emergency response and life-saving operations during the first hours following a disaster. Decision-makers rely heavily on near-real-time information about the spatial distribution of ground shaking and its expected consequences for the built environment in order to prioritize search-and-rescue activities and allocate emergency resources. In many operational systems, this information is derived from ShakeMap-based ground-motion fields combined with building vulnerability models to produce rapid estimates of earthquake-induced damage. However, the reliability of these estimates depends strongly on how accurately the ShakeMap representation captures local site effects and basin-related amplification. In deep-basin urban environments, where seismic waves may be amplified within thick sedimentary deposits, scenario-based ShakeMaps may underestimate spectral demand. Such underestimation may propagate into damage estimation results and potentially lead to operational damage misclassification during the early phase of emergency response. In this study, operational damage misclassification is defined as the misallocation of emergency response priorities caused by biased ground-motion representation in rapid damage estimation frameworks. Accordingly, this study investigates how scenario-based ShakeMap representations in deep-basin urban environments may induce such misclassification.

In the disaster risk literature, the period commonly referred to as the “Golden Hours”—the first 72 hours following a major earthquake—is widely recognized as a critical time window for reducing loss of life (Li and Xu, 2025; Li et al., 2023). During this period, the rapid identification of trapped individuals, the assessment of the safety condition of the building stock, and the implementation of effective evacuation decisions depend on the availability of high-resolution, spatially distributed information on expected building damage derived from earthquake ground shaking. Multi-level building damage classification frameworks enable response strategies to be formulated on a rational basis by providing search-and-rescue teams with an initial, model-based representation of damage severity across the affected area, while also facilitating the deployment of personnel and equipment with appropriate capacity and characteristics to the affected areas.

Previous studies have demonstrated that a time gain of approximately 6–12 hours in post-earthquake damage assessment can substantially improve rescue outcomes, highlighting the critical importance of rapid and automated damage classification approaches (Erdik et al. 2011;Li and Xu 2025).

Accordingly, near-real-time damage estimation systems that become operational immediately after an event have emerged as a cornerstone of contemporary disaster management. Such platforms aim to provide decision-makers with early, spatially explicit estimates of earthquake-induced ground shaking and potential impacts, thereby supporting the prioritization of response actions during the initial phase. Representative implementations include HAZUS (FEMA, 2025) , ELER (Hancilar et al., 2010) , PAGER (Wald et al., 2010) , SELENA (NORSAR and ICG 2026), OpenQuake (Silva et al., 2013) , AFAD-RED (AFAD, 2013), and REDAS (REDAS, 2020).

Despite their operational value, the reliability of rapid post-event damage products is fundamentally constrained by the accuracy of the underlying ground-shaking representation and the resulting damage estimation outputs. To enable immediate

https://doi.org/10.5194/egusphere-2026-1523
Preprint. Discussion started: 10 April 2026

assessments, most operational systems rely on scenario-based, event-specific ShakeMaps derived from regional site parameters (e.g., V_{s30}, $Z_{1.0}$, $Z_{2.5}$) and Ground Motion Prediction Equations (GMPEs), combined with fragility functions representing the building stock. While this framework facilitates rapid computation and coordinated response planning, it inevitably introduces both epistemic and aleatory uncertainties. Consequently, a persistent methodological gap may emerge between pre-event scenario-based projections and post-event damage patterns governed by the actual ground-motion field and observed impacts. In complex deep-basin urban environments, where amplification effects may distort intermediate-period demand, this gap can become particularly pronounced, complicating the balance between timeliness and representational accuracy in early-phase decision support.

Beyond these methodological constraints, existing research has predominantly evaluated system performance in terms of statistical prediction accuracy and bias reduction in ground-shaking and loss estimation (e.g., Silva et al. 2025). While previous studies have demonstrated that observational calibration improves ground-motion and damage model reliability, limited attention has been paid to how scenario-based ShakeMaps influence exceedance probabilities of operationally critical cumulative damage thresholds during the “Golden Hours”. In deep-basin urban environments, where basin-induced amplification may alter intermediate-period spectral demand, optimistic bias in scenario-based ground-shaking representations may systematically underestimate exceedance probabilities associated with severe damage states. Such underestimation does not merely constitute a modelling discrepancy; rather, it may assign affected areas to a lower operational response regime than warranted, thereby inducing governance-level misclassification during the early phase of emergency management. Operational misclassification refers to the assignment of affected areas to a lower response category due to underestimation of cumulative damage exceedance probabilities. The explicit linkage between ShakeMap-driven damage exceedance probabilities and operational response thresholds has received comparatively limited attention in the disaster risk science literature.

The primary objective of this study is to quantify how scenario-based ShakeMaps may influence the estimation of exceedance probabilities for operationally critical cumulative damage thresholds, and to evaluate how station-based updating modifies these probabilities during the golden hours. Using the 30 October 2020 Samos earthquake as a case study, with a focus on the deep-basin urban context of Bayraklı, Izmir, a two-stage framework is implemented: (i) a scenario-based ground-shaking representation and (ii) a station-updated calibration using spatially proximal strong-motion records. By benchmarking both stages against observed damage patterns and building inventory data, the study isolates the extent to which underestimation of exceedance probabilities may translate into governance-level misclassification within early-phase emergency response planning.

This study contributes to disaster risk science by reframing ShakeMap-driven damage estimation within a governance-level misclassification perspective. Rather than focusing solely on statistical accuracy improvements, it demonstrates how underestimation of exceedance probabilities for operationally critical cumulative damage thresholds may shift affected areas into lower response regimes during the golden hours. By explicitly linking scenario-based ShakeMap bias to operational

https://doi.org/10.5194/egusphere-2026-1523
Preprint. Discussion started: 10 April 2026

response escalation, the study highlights the strategic importance of near-real-time station updating in reducing early-phase misclassification risk in deep-basin urban environments.

2 Study Area and Seismotectonic Setting

The Samos earthquake, which occurred offshore of Samos Island, Greece, on 30 October 2020 at 11:51:27 local time, represents a key reference event for earthquake engineering studies in Türkiye, primarily due to the distinct and spatially heterogeneous damage pattern observed in the affected regions. The moment magnitude of the earthquake was reported as Mw = 6.6 by the Disaster and Emergency Management Authority of Türkiye (AFAD, 2020), Mw = 6.9 by the Kandilli Observatory and Earthquake Research Institute,(KOERI, 2020) and Mw = 7.0 by the United States Geological Survey (USGS, 2020). The slight variability among reported moment magnitude values reflects epistemic uncertainty in source characterization, which may propagate into scenario-based ground-motion simulations used in rapid damage estimation frameworks.

The seismotectonic setting of the eastern Aegean region is governed by a dominant extensional regime associated with the north–south opening of the Aegean Sea. This tectonic environment is characterized by widespread normal faulting, accommodating crustal thinning and producing moderate-to-large magnitude earthquakes (Kiratzi et al., 2021;Askan et al., 2021). The earthquake was generated by normal faulting on an east–west trending offshore fault system consistent with the regional extensional tectonic regime of the eastern Aegean. A defining characteristic of the event was the disproportionate concentration of severe structural damage and casualties in the Bayraklı district of Izmir (Türkiye), despite its distance of approximately 76 km from the epicenter, highlighting the role of thick Quaternary alluvial deposits (Demirel et al., 2022; Tuna, 2026).

Although structural deficiencies related to design, detailing, and construction practices contributed to the observed damage (METU EERC, 2020; DAUM, 2020) one of the primary factors governing the the spatial concentration of damage in Bayraklı has been widely attributed to the combined influence of local site response effects and structural vulnerability. Crucially, the geotechnical and geological characteristics of the Izmir Bay basin played a decisive role in shaping the observed damage distribution. Specifically, the partial trapping and amplification of seismic waves within deep and soft alluvial deposits increased ground-motion amplitudes and extended the duration of strong shaking, thereby imposing elevated seismic demands on the local building stock (Cetin et al., 2022).

The densely populated northern, eastern, and southern shores of the inner Izmir Bay are bordered by the Menemen, Bornova, and Yeşildere plains, which are characterized by deep alluvial deposits. These plains are constrained by elevated topography composed predominantly of bedrock outcrops, creating a sharp geological contrast with the basin sediments. This geological configuration underscores that Izmir, and the Bayraklı district in particular exhibits distinct, site-specific geotechnical characteristics. Consequently, seismic hazard assessment based solely on standardized code-based approaches is insufficient;

instead, detailed microzonation studies are imperative to adequately capture local site effects and basin-induced ground-motion amplification (Demirel et al., 2022) .

To comprehensively understand and evaluate the seismic impact, several studies have utilized acceleration records from AFAD strong-motion stations to compute 5%-damped acceleration response spectra. These spectra were subsequently benchmarked against the design spectra prescribed in successive Turkish seismic codes, including the Code for Structures to be Constructed in Disaster Areas (CSCDA 1975 and 1997), the Code for Buildings to be Constructed in Seismic Areas (CBCSA 2007), and the Turkish Building Earthquake Code (TBEC 2018). In this context, (Yakut et al., 2021) focused on spectral comparisons specific to the Turkish regulatory framework. Expanding this scope,(Askan et al., 2021) compared the spectral content with Greek seismic codes (EAK, 2000), (Eurocode 8) and conducted a joint evaluation of strong-motion records from both countries.

Comparative analyses across the Izmir Bay region indicate that, despite pronounced long-period amplifications observed at certain sites, the response spectra of the recorded ground motions generally remained below the design envelopes prescribed by both current and former Turkish seismic codes. This observation suggests that structural vulnerabilities and variations in code implementation and construction quality contributed significantly to the observed damage, in combination with local site amplification effects. In particular, in the Bayraklı district, the occurrence of structural collapse and severe damage under ground motions generated by an earthquake located approximately 70 km away underscores the substantial role of structural and construction-related deficiencies (Askan et al., 2021).

These basin-related amplification characteristics are particularly relevant for exceedance-based damage assessment frameworks. Amplification of intermediate-period spectral demand may substantially influence cumulative damage probabilities, even in cases where peak ground acceleration values do not appear extreme. In such settings, scenario-based ShakeMaps that do not fully capture basin-induced effects may underestimate exceedance probabilities associated with operationally critical damage thresholds. Consequently, deep-basin urban environments provide a suitable context for examining how representational bias in ground-shaking fields may translate into governance-level misclassification during the early response phase.

The predictive performance of contemporary Ground Motion Prediction Equations (GMPEs) for the 2020 Samos earthquake has also been critically examined in the literature (Gülerce et al., 2022), demonstrating that model-based ground-motion representations may not fully capture the spatial variability of recorded ground motions in basin-affected regions.

3 Methodology

A two-stage evaluation framework was implemented to assess the impact of station-based updating on event-specific ground-motion representation and damage estimation, as illustrated in Figure 1. In Stage 1, deterministic scenario-based ShakeMaps were generated using the earthquake source parameters of the 30 October 2020 Samos earthquake, regional site conditions represented by the Vs30 map, and bedrock depth parameters ($Z_{1.0}$ and $Z_{2.5}$). Ground-motion parameters were estimated using a set of established Ground Motion Prediction Equations (GMPEs). While GMPEs provide statistically robust estimates of expected ground motion, their ability to accurately represent spatial variability for a specific event remains inherently constrained due to their empirical formulation (Zhao et al., 2023).

160

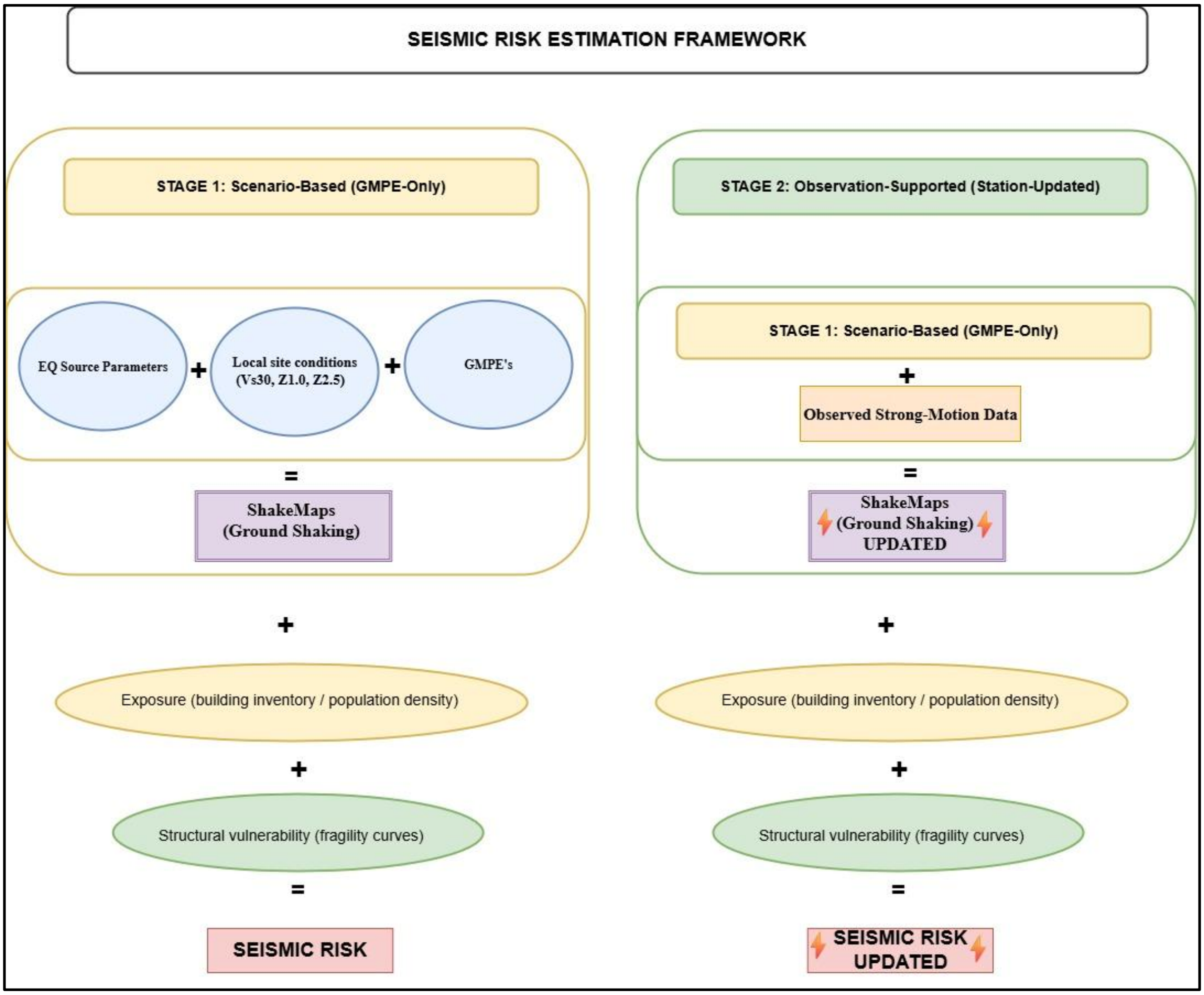

Figure 1. Two-stage framework for rapid and station-updated seismic hazard and risk estimation

Within this two-stage framework, the primary decision-relevant metric is defined as the exceedance probability of cumulative damage states (e.g.,{M+E+C}), rather than absolute damage counts, as these probabilities directly inform operational response thresholds during the early phase of emergency management. 165

Based on the resulting ground-motion representation, theoretical damage distributions were derived by combining the ShakeMaps with fragility curves representing different building classes within the study area. These scenario-based damage estimates were subsequently evaluated in terms of cumulative damage exceedance probabilities and contrasted with observed post-earthquake damage patterns to assess how the purely model-driven representation may influence operational threshold classification. Accordingly, this scenario-based model serves as the baseline ground-motion representation against which cumulative damage exceedance probabilities are subsequently evaluated in Stage 2.

In Stage 2, a station-updated approach was implemented by incorporating strong-motion records from the AFAD seismic network associated with the Samos earthquake. The ShakeMaps generated in Stage 1 were updated through bias correction using observed ground-motion parameters recorded at station locations. The seismic risk analysis was then repeated within the same methodological framework, and the resulting damage distributions were re-evaluated in terms of cumulative damage exceedance probabilities.

This two-stage comparison enables the quantification of how station-based updating modifies exceedance probabilities associated with operationally critical cumulative damage thresholds, and consequently how scenario-based representations may influence operational response categorization during the early response phase.

Strong-motion station monitoring networks therefore provide not only empirical validation of ground-motion levels, but also a mechanism for reducing uncertainty in exceedance-based damage assessment and associated response categorization (Silva et al., 2025).

3.1. Selection of Ground Motion Prediction Equations (GMPEs)

The selection of Ground Motion Prediction Equations (GMPEs) is a critical factor influencing the representation of spectral demand in seismic hazard and risk analyses. Because GMPEs empirically integrate earthquake source characteristics, wave propagation effects, and local site conditions to estimate ground-motion levels, their selection directly affects the resulting exceedance probabilities associated with cumulative damage states. Consequently, it is essential that the selected model set is appropriate for both the tectonic environment of the study area and the earthquake type under consideration.

Previous studies widely recognized in the literature have demonstrated that models developed within the global Next Generation Attenuation (NGA) framework—particularly NGA-West 1 (Power et al., 2008) and NGA-West 2 (Bozorgnia et al., 2014) exhibit satisfactory performance in predicting strong ground motions recorded in Türkiye (Gülerce et al., 2022). Accordingly, four GMPEs developed as part of the NGA-West 2 project, ASK14 (Abrahamson et al., 2014) BSSA14 (Boore et al., 2014), CB14 (Campbell and Bozorgnia, 2014), and CY14 (Chiou and Youngs, 2014) - were selected for this study. These models were incorporated with equal weighting in the hazard analysis. The selected model set is also consistent with the development philosophy of the European Seismic Hazard Model (ESHM) (EFEHR, 2026).

Nevertheless, the application of these models in regions characterized by complex basin geometry, such as the Izmir Bay, requires particular caution. Detailed analyses of strong-motion recordings indicate that empirical constraints embedded in GMPE formulations to represent site and basin amplification effects are inherently case-dependent and may not fully capture region-specific amplification patterns (Day et al., 2008). In exceedance-based damage assessment, such representational limitations may propagate into cumulative damage probabilities and influence operational response categorization. For this reason, the GMPE-based ground-motion predictions obtained in Stage 1 were subsequently reassessed and updated in Stage

2 using observed station recordings, allowing region-specific site and basin effects to be explicitly incorporated into the final exceedance-oriented seismic risk evaluation.

3.2. Characterization of Local Site Conditions

The accurate parameterization of local site conditions is a prerequisite for the consistent representation of spectral demand within Ground Motion Prediction Equation (GMPE)-based hazard frameworks. Because GMPE formulations integrate earthquake source characteristics, wave propagation effects, and site conditions through empirical relationships, uncertainties in site characterization may directly influence predicted response spectra and, consequently, cumulative damage exceedance probabilities.

The primary parameter used for site characterization is the shear-wave velocity in the upper 30 m (V_{s30}). The spatial distribution of V_{s30} was derived through multi-source data integration. As a baseline, the “Topographic Slope as a Proxy for Seismic Site Conditions” dataset provided by the USGS (USGS, 2023) was adopted. This regional model was subsequently refined using locally derived V_{s30} estimates obtained from available geotechnical borehole logs within the study area . The resulting V_{s30} distribution was further evaluated through comparison with equivalent shear-wave velocity contour maps produced for the Izmir Metropolitan Municipality as part of the “Izmir Earthquake Scenario and Earthquake Master Plan” project (Izmir Metropolitan Municipality and Boğaziçi University 1999) and illustrated with Figure 2. This comparison provided an additional level of confidence regarding the spatial consistency and representativeness of the adopted site condition model for subsequent hazard and risk analyses. Given that V_{s30} strongly controls amplification behavior in empirical GMPE formulations, spatial variability in this parameter directly affects exceedance-based damage estimation and associated response categorization. All spatial visualizations were produced using QGIS software (QGIS.org, 2024) (QGIS.org, 2024).

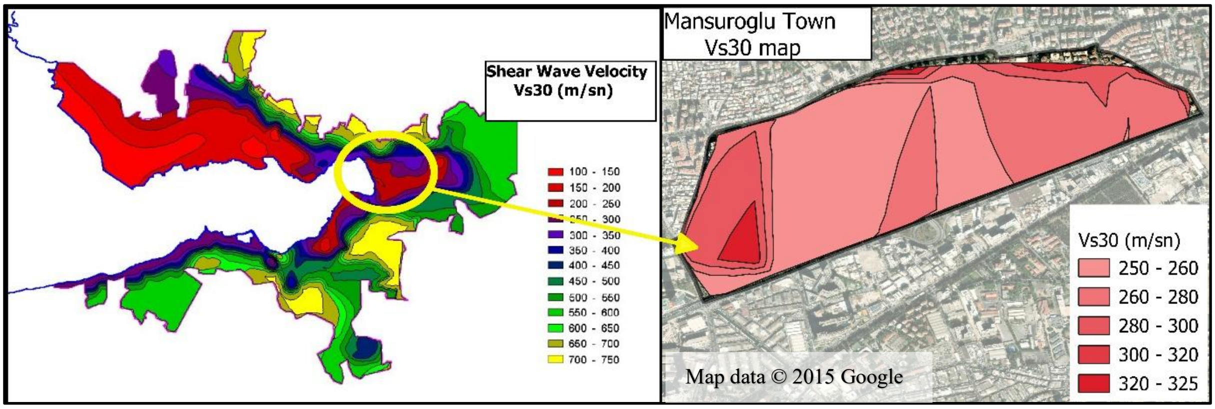

Figure 2. Spatial distribution of local site conditions based on Vs30. The regional Vs30 map for the Izmir Bay area (left panel) is adopted from the Izmir Earthquake Scenario and Master Plan (1999). Base map source: © Google Maps 2015 (retrieved via QGIS QuickMapServices).

To represent site amplification and basin effects in seismic wave propagation, Ground Motion Prediction Equations (GMPEs) require, in addition to the V_{s30} parameter, sediment depth proxies namely $Z_{1.0}$ (depth to V_S=1.0 km/s) and $Z_{2.5}$

https://doi.org/10.5194/egusphere-2026-1523
Preprint. Discussion started: 10 April 2026

(depth to V_S=2.5 km/s). Because the direct measurement of these depth parameters is not feasible for most sites, they are commonly estimated using empirical relationships reported in the literature.

It is well recognized that, particularly in regions characterized by deep and complex basin geometries, uncertainties associated with the empirical estimation of $Z_{1.0}$ and $Z_{2.5}$ may lead to systematic deviations in the modelling of long-period ground-motion demands. In deep-basin environments, uncertainties in sediment depth proxies may disproportionately influence intermediate-period spectral demand, thereby altering cumulative damage exceedance probabilities even in the absence of extreme peak ground acceleration values.

Due to the limited availability of deep borehole data reaching bedrock within the study area, $Z_{1.0}$ and $Z_{2.5}$ were derived from V_{s30} values using the empirical relationships developed within the NGA-West 1 project (Askan et al., 2021). Accordingly, these parameters were calculated using Eq. ((1) and Eq. ((2), respectively.

In regions underlain by deep alluvial basins, such as the Izmir Bay, the accurate characterization of sediment depth parameters (e.g., $Z_{1.0}$ and $Z_{2.5}$) is essential for ensuring the reliability and representativeness of seismic hazard assessments. Investigations conducted for the 2020 Samos earthquake indicate that districts such as Bayraklı and Karşıyaka, characterized by predominant site periods in the range of 1.0–3.0 s, exhibited pronounced amplification of spectral accelerations, particularly within the 0.5–1.5 s period range(Cetin et al., 2022).

$$ln(Z_{1.0}) = \begin{cases} 6.745 & for\ V_{s30} < 180\ m/sn \\ 6.745 - 1.35 * ln(\frac{V_{s30}}{180}) & for\ 180 \leq V_{s30} \leq 500\ m/sn \\ 5.394 - 4.48 * ln(\frac{V_{s30}}{500}) & for\ V_{s30} \geq 500\ m/sn \end{cases} \quad \textbf{(1)}$$

$$Z_{2.5} = 0.519 + 3.595 * Z_{1.0} \quad \textbf{(2)}$$

These observations reported in the literature suggest that standard Ground Motion Prediction Equations (GMPEs) may not adequately represent basin-induced amplification effects and long-period ground-motion characteristics, especially under deep sedimentary basin conditions. Consequently, in this study, the refinement of ground-motion estimates initially derived from theoretically defined site and basin parameters using observed strong-motion station data was adopted through bias correction, not as an optional enhancement, but as a methodological requirement to improve hazard and risk representation.

3.3. Fragility Curves and Building Inventory

One of the most critical components of seismic risk analysis is the ability of fragility curves to represent the probabilistic relationship between ground-motion intensity measures (e.g., PGA, spectral acceleration) and the likelihood of exceeding predefined physical damage states within the regional building stock. In exceedance-based risk evaluation, these curves provide the basis for estimating cumulative damage probabilities associated with operationally relevant threshold levels. In this study, HAZUS-based (FEMA, 2025) fragility curves were adopted due to their widespread use in the literature and broad acceptance in engineering applications.

Figure 3 illustrates the location of the Samos earthquake, its spatial relationship to the Mansuroğlu Neighborhood, and the distribution of earthquake-damaged buildings across the neighborhood according to damage severity levels. The building inventory for the Mansuroğlu Neighborhood (Bayraklı District, Izmir) was obtained from the Republic of Türkiye Ministry of Environment, Urbanization and Climate Change, General Directorate of Construction Affairs. The dataset was subsequently harmonized with the HAZUS building classification scheme by considering key attributes such as structural system type, number of stories, and level of engineering design. Although originally developed for the United States building stock, HAZUS fragility functions were adopted in this study due to their broad representation of structural typologies and their widespread use in international seismic risk assessments.

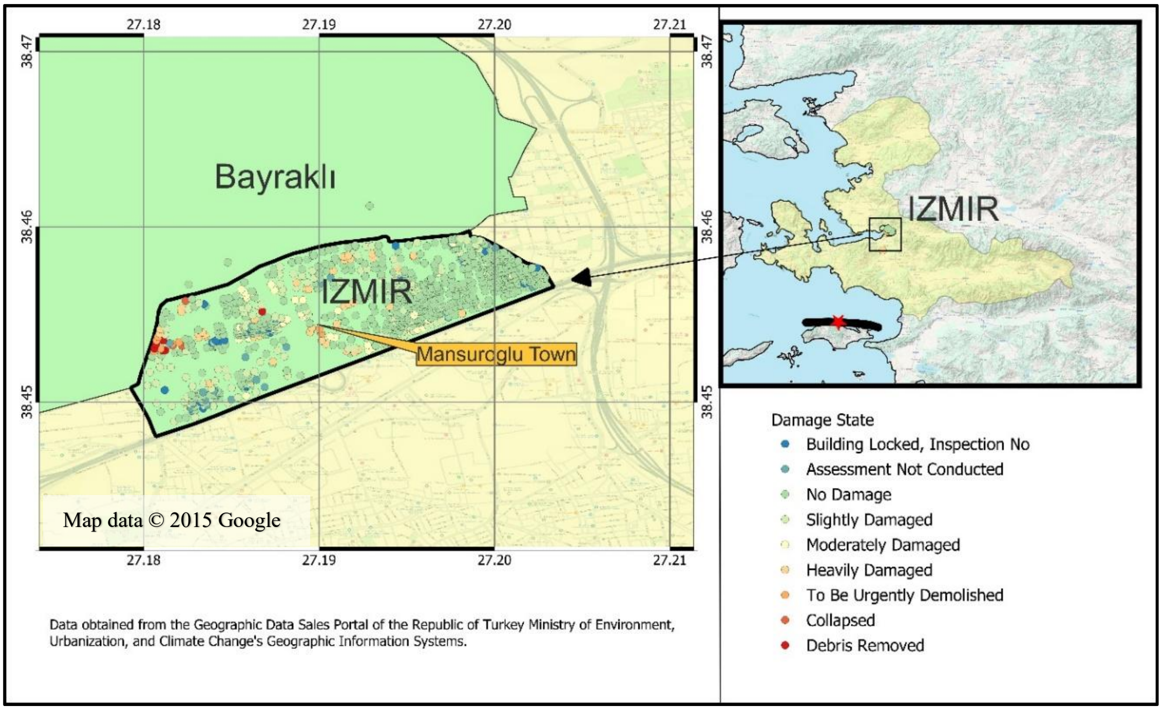

Data obtained from the Geographic Data Sales Portal of the Republic of Turkey Ministry of Environment, Urbanization, and Climate Change's Geographic Information Systems.

Figure 3. Location of the 30 October 2020 Samos earthquake and spatial distribution of observed building damage in the Mansuroğlu Neighborhood, Izmir. Base map source: © Google Maps 2015 (retrieved via QGIS QuickMapServices).

The compiled dataset consists of 962 buildings, for which post-earthquake damage information from the 30 October 2020 Samos earthquake is available. The inventory indicates that the building stock is predominantly composed of reinforced concrete (RC) frame structures (92.5%), reflecting the typical mid- to high-rise residential building typology of Izmir (Yakut et al., 2021). A small fraction of the stock consists of masonry buildings, while structural system information is unavailable for approximately 5.6% of the buildings.

https://doi.org/10.5194/egusphere-2026-1523
Preprint. Discussion started: 10 April 2026

In terms of height distribution, the inventory is dominated by mid-rise buildings (4–7 stories, 48.3%) and high-rise buildings (≥8 stories, 36.7%), whereas low-rise buildings (1–3 stories) constitute 13.5% of the stock. This distribution suggests that seismic demand and site-related amplification effects are likely to be particularly relevant for the mid- and high-rise building groups. Given the concentration of mid- and high-rise reinforced concrete buildings, intermediate-period spectral demand amplification may exert a disproportionate influence on cumulative damage exceedance probabilities in the study area.

Construction year's information represents a major source of uncertainty in the available inventory, as it is unknown for 56.1% of the buildings. Structures with known construction years were classified according to the evolution of Turkish Earthquake Design Codes as Pre-Code (pre-1975), Low-Code (1975–1996), Moderate-Code (1997–2007), High-Code (2008–2018), and Very High-Code (post-2018). For buildings with missing construction year information, a conservative Low-Code assumption was adopted to avoid underestimation of seismic risk. This conservative assumption was adopted to reduce the risk of downward bias in cumulative damage exceedance estimation resulting from incomplete inventory data.

Post-earthquake field investigations following the Samos earthquake indicate that damage in Bayraklı was concentrated primarily in 7–9-story reinforced concrete moment-resisting frame buildings, often constructed without shear walls (DAUM,2020). Accordingly, reinforced concrete buildings were classified under the C1 (Concrete Moment Frame) category and further subdivided based on building height as C1L (low-rise, 1–3 stories), C1M (mid-rise, 4–7 stories), and C1H (high-rise, ≥8 stories), where the suffixes L, M, and H denote low-, mid-, and high-rise structural configurations, respectively. Classification of the building inventory according to structural type, height class, and assumed seismic design level is illustrated with Figure 4.

For buildings with unknown structural system information, a hybrid classification strategy was employed. Buildings with four or more stories were assumed to behave as reinforced concrete frame structures, consistent with regional construction practices, but were conservatively assigned a Low-Code design level (C1M-2 or C1H-2) to explicitly account for uncertainty.

In this classification scheme, the numerical suffix denotes the assumed seismic design level, where "-1" corresponds to Pre-Code, "-2" to Low-Code, "-3" to Moderate-Code, "-4" to High-Code, and "-5" to Very High-Code buildings constructed in accordance with post-2018 seismic regulations.

In contrast, low-rise buildings (1–3 stories) with unknown structural systems, as well as masonry buildings, were considered unsuitable for spectral-demand-based fragility assessment due to the inability to reliably characterize their structural behavior. These structures were therefore evaluated using intensity-based fragility functions under the BI000 classification.

The adopted classification and fragility assignment strategy aims to limit the influence of incomplete inventory data on the seismic risk analysis while maintaining a transparent and methodologically defensible framework for exceedance-based damage estimation and subsequent operational response interpretation.

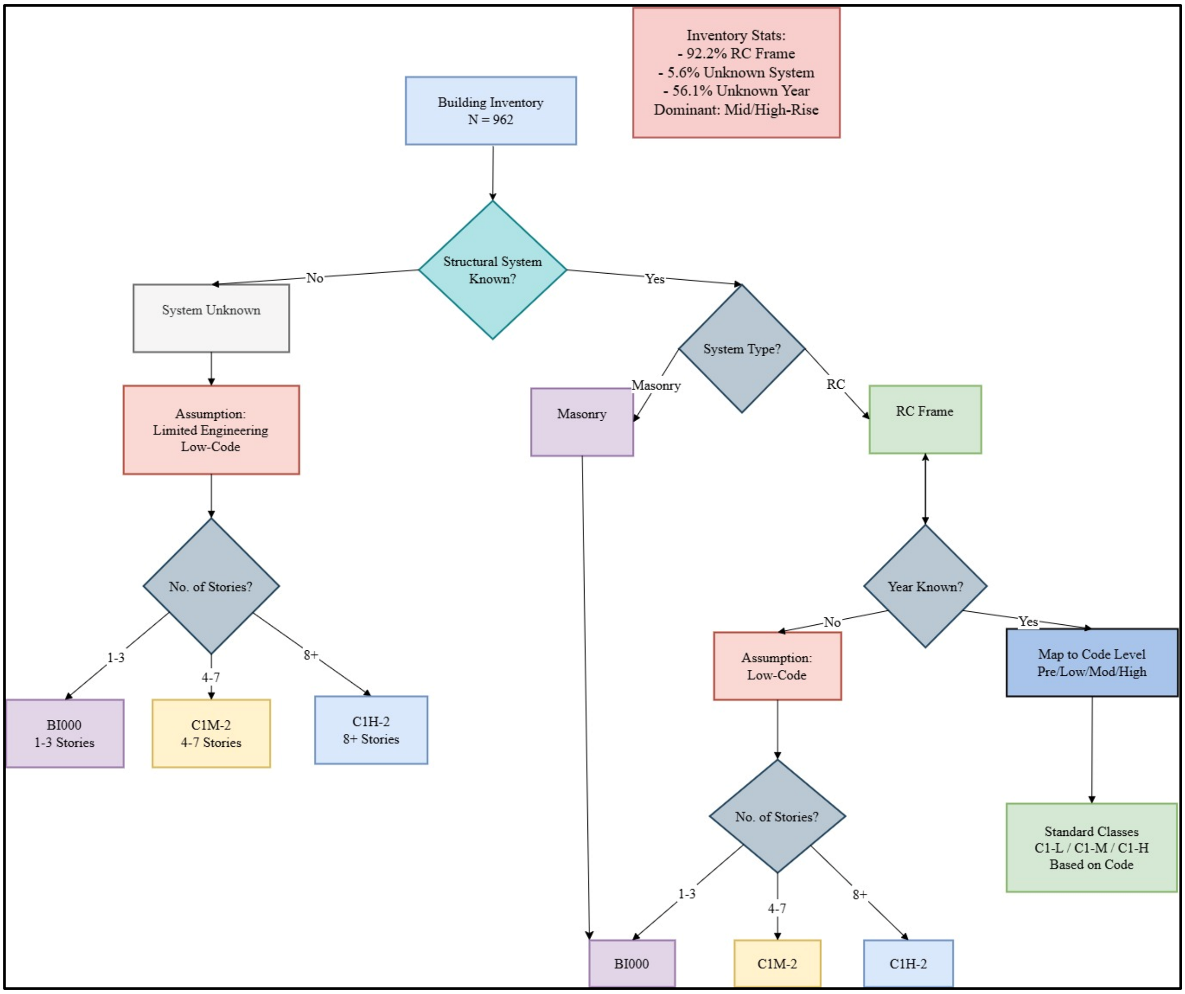

Figure 4. Classification of the building inventory according to structural type, height class, and assumed seismic design level

4 Results and Discussion

This section presents the results of the rapid (Stage 1) and station-updated near-real-time (Stage 2) damage estimation analyses conducted for the Izmir–Bayraklı–Mansuroğlu region during the 30 October 2020 Samos earthquake. The discussion is structured around the two-stage framework defined in the Methodology section, with emphasis on how station-based updating modifies the ground-motion representation and propagates into cumulative damage exceedance patterns that are operationally relevant for early-phase decision support.

4.1. Comparison of Station Records and Grid-Based Ground-Motion Estimation at Station Locations

To evaluate how station-based updating alters the event-specific ground-motion representation, three datasets were compared at AFAD strong-motion station locations: (i) recorded observations, (ii) scenario-based (Stage 1) estimates extracted from the nearest grid centroids, and (iii) station-updated (Stage 2) estimates after bias correction. This station-level comparison provides a consistency check for the updating procedure and establishes the basis for interpreting how local representational differences may influence spatial ShakeMaps and exceedance-based damage estimates in subsequent sections. All AFAD strong-motion stations located within a 3.0 km radius of the Mansuroğlu Neighborhood (n = 4) were included in the comparison, ensuring full utilization of the available observational data in the immediate vicinity of the study area. The station identifiers, locations, earthquake parameters obtained from AFAD TADAS (https://tadas.afad.gov.tr), and corresponding spectral acceleration plots are presented in Figure 5.

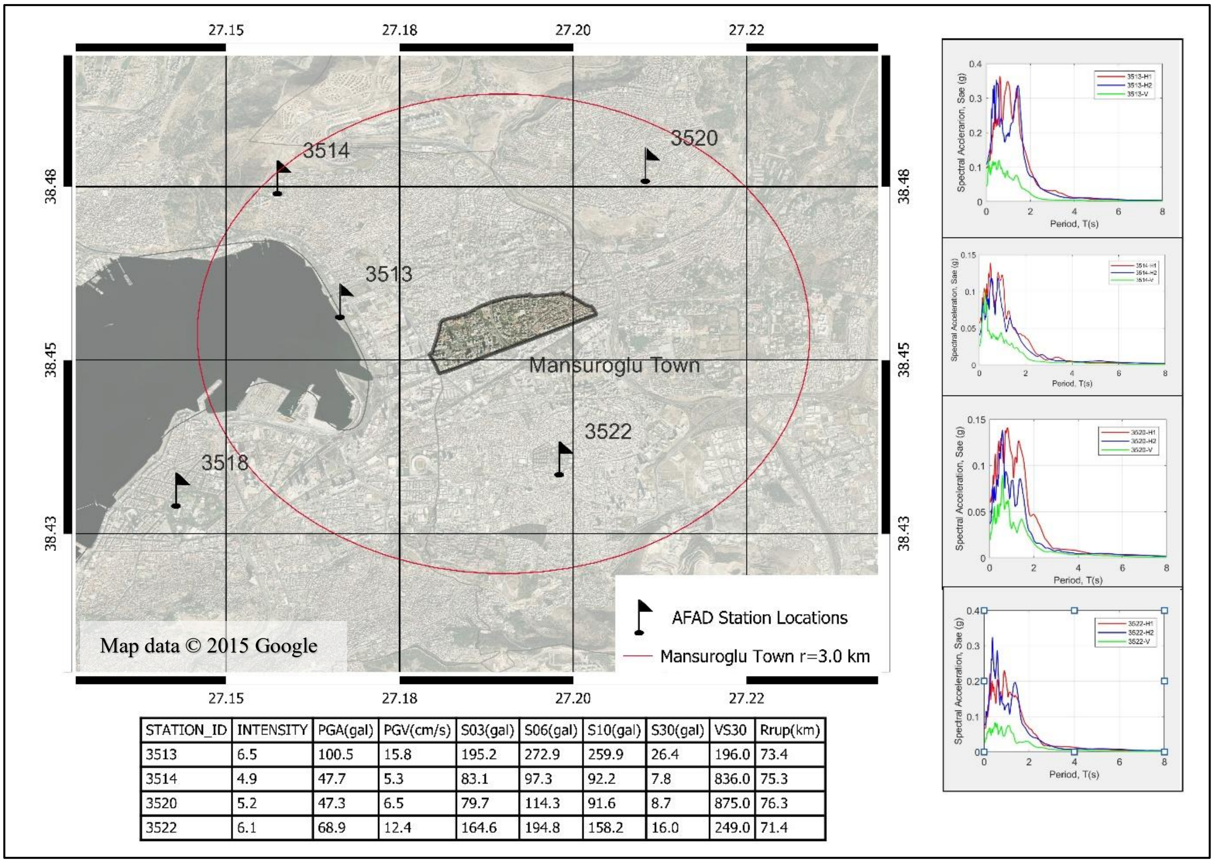

STATION_ID	INTENSITY	PGA(gal)	PGV(cm/s)	S03(gal)	S06(gal)	S10(gal)	S30(gal)	VS30	Rrup(km)
3513	6.5	100.5	15.8	195.2	272.9	259.9	26.4	196.0	73.4
3514	4.9	47.7	5.3	83.1	97.3	92.2	7.8	836.0	75.3
3520	5.2	47.3	6.5	79.7	114.3	91.6	8.7	875.0	76.3
3522	6.1	68.9	12.4	164.6	194.8	158.2	16.0	249.0	71.4

Figure 5. AFAD strong-motion station locations and observed ground-motion parameters. Base map source: © Google Maps 2015 (retrieved via QGIS QuickMapServices).

https://doi.org/10.5194/egusphere-2026-1523
Preprint. Discussion started: 10 April 2026

The effect of station-based updating on ground-motion representation is summarized in Table 1. Improvement was quantified using an absolute error–based approach, comparing scenario-based (Stage 1) and station-updated (Stage 2) estimates against observed AFAD strong-motion records.

Table 1. Comparison of observed and scenario-based ground-motion parameters with station-calibrated estimation, and corresponding improvement ratios for selected AFAD strong-motion stations.

Station ID	Data Type	PGA (cm/s^2)	$S_{0.3}$ (cm/s^2)	$S_{0.6}$ (cm/s^2)	$S_{1.0}$ (cm/s^2)	$S_{3.0}$ (cm/s^2)
3513	Observed Data	100.51	195.17	272.92	259.9	26.44
	Scenario-Based SHA	70.3	209.82	176.81	102.44	25.68
	Calibrated SHA	77.17	209.21	211.52	158.72	26.36
	Improvement (%)	*22.70%*	*4.16%*	*36.11%*	*35.70%*	*89.50%*
3514	Observed Data	47.74	83.1	97.26	92.21	7.77
	Scenario-Based SHA	40.17	76.62	52.13	25.95	6.06
	Calibrated SHA	44.79	77.36	67.93	48.87	6.5
	Improvement (%)	*61.00%*	*11.42%*	*35.01%*	*34.60%*	*25.70%*
3520	Observed Data	47.35	79.66	114.26	91.57	8.68
	Scenario-Based SHA	38.8	72.89	49.4	24.53	5.78
	Calibrated SHA	41.06	74.71	66.03	41.75	6.52
	Improvement (%)	*26.40%*	*26.88%*	*25.64%*	*25.70%*	*25.50%*
3522	Observed Data	68.86	164.55	194.78	158.15	15.95
	Scenario-Based SHA	68.04	191.7	155.66	87.67	21.34
	Calibrated SHA	68.85	184.62	167.32	108.17	19.99
	Improvement (%)	*98.80%*	*26.08%*	*29.81%*	*29.10%*	*25.00%*

In the analyses, observed ground-motion parameters derived from AFAD strong-motion station records were used as reference values (Observed) for the evaluation of both uncalibrated and calibrated ground-motion estimation.

The pre-calibration absolute error ($\mathrm{AE}_{\mathrm{est}}$) was defined as the absolute difference between observed and scenario-based estimates (Eq. ((**3**)), whereas the post-calibration error ($\mathrm{AE}_{\mathrm{cal}}$) was computed analogously for the updated ShakeMaps (Eq. ((**4**)).

$$AE_{est} = | \; Observed - Estimated \; | \tag{3}$$

$$AE_{cal} = | \; Observed - Calibrated \; | \tag{4}$$

The relative reduction in absolute error due to calibration was expressed with (**5**:

$$Improvement(\%) = \frac{AE_{est} - AE_{cal}}{AE_{est}} \times 100 \tag{5}$$

Positive Improvement (%) (Eq. **5**) values indicate reduced station-level representational bias following calibration. Across the four stations, the most pronounced improvements are observed in the intermediate-period range (T=0.6–1.0 s), where relative error reductions frequently exceed 25–35%. This period band is particularly relevant for mid- to high-rise reinforced concrete buildings that dominate the study area and later govern cumulative damage exceedance patterns discussed in Section 4.3.

4.2. Comparative Analysis of Scenario-Based and Station-Calibrated Hazard Estimation

This section compares the spatial ground-motion representations obtained under the scenario-based (Stage 1) and station-calibrated (Stage 2) configurations for the Mansuroğlu Neighborhood during the 30 October 2020 Samos earthquake. The objective is not merely to contrast hazard amplitudes, but to evaluate how observational updating reshapes the spatial distribution of spectral demand in period ranges that govern structural response.

In Stage 1, PGA and spectral accelerations at 0.3 s, 0.6 s, 1.0 s, and 3.0 s were derived exclusively from earthquake source parameters, regional site conditions, and GMPE-based predictions. In Stage 2, these ShakeMaps were bias-corrected using AFAD strong-motion recordings while preserving identical grid resolution and classification intervals to ensure direct spatial comparability. As shown in Figure 6, the integration of station data results in a moderate upward shift in dominant PGA levels, from approximately 60–65 cm/s² to 65–75 cm/s².

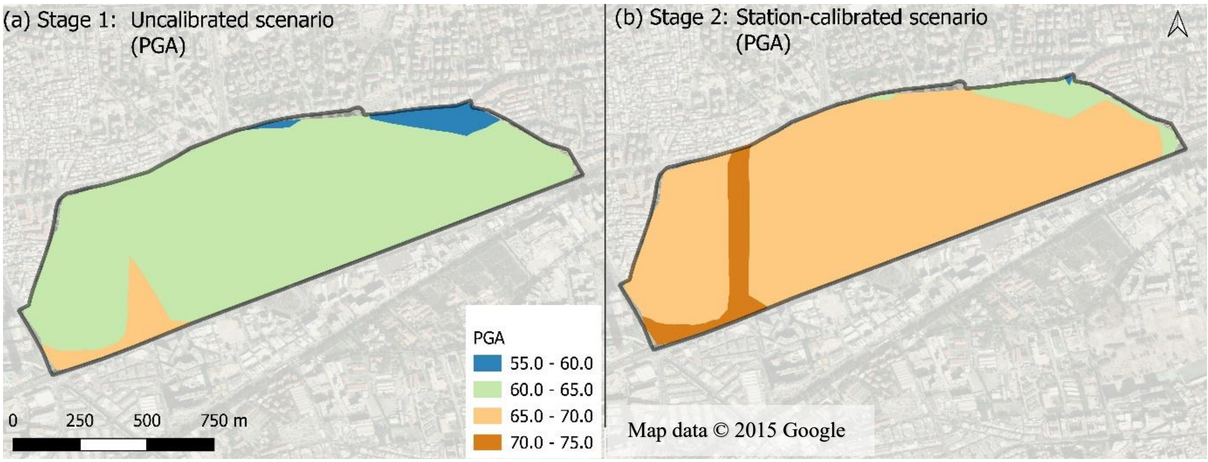

Figure 6. Comparison of Stage 1 (scenario-based) and Stage 2 (station-calibrated) PGA ShakeMaps for the Mansuroğlu Neighborhood. Base map source: © Google Maps 2015 (retrieved via QGIS QuickMapServices).

https://doi.org/10.5194/egusphere-2026-1523
Preprint. Discussion started: 10 April 2026

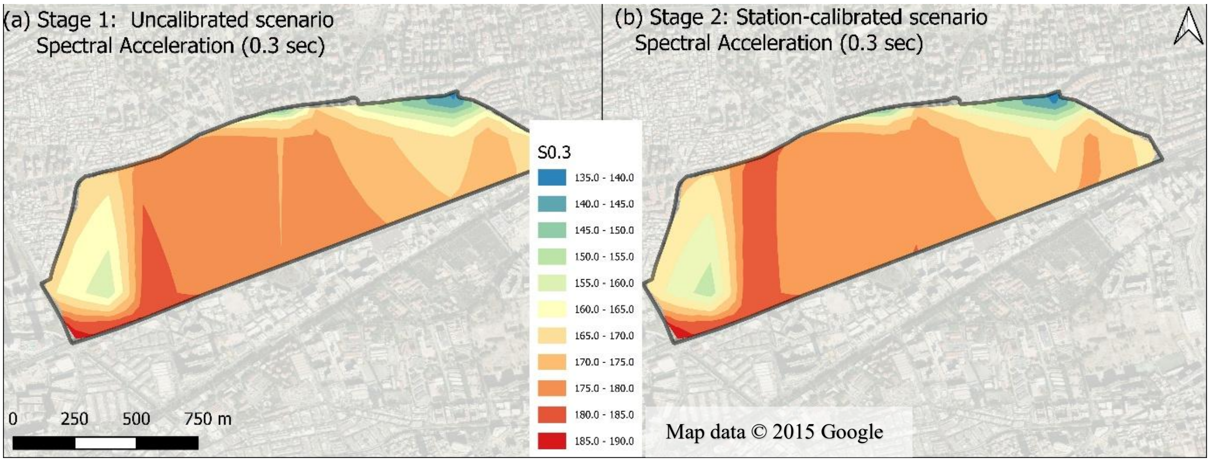

Figure 7. Comparison of Stage 1 (scenario-based) and Stage 2 (station-calibrated) Sa (T = 0.3 s) ShakeMaps for the Mansuroğlu Neighborhood. Base map source: © Google Maps 2015 (retrieved via QGIS QuickMapServices).

Although the amplitude differences remain limited, this shift indicates localized deviations from purely scenario-based GMPE estimates. Figure 7 displays spatial patterns of Sa (T = 0.3 s) broadly consistent with the PGA distribution. Differences between Stage 1 and Stage 2 remain relatively modest, indicating that short-period spectral demand is less sensitive to basin-related representational bias in this case.

A more substantial divergence emerges in the intermediate-period band, which is critical for the urban character of the study area. As illustrated in Fig. 8 and Fig. 9, the station-calibrated configuration (Stage 2) reveals significantly stronger and more spatially concentrated amplification zones compared to the scenario-based representation (Stage 1) for T = 0.6s and T = 1.0s. The results indicate that Stage 1 systematically underestimates spectral demand in this range, particularly in zones underlain by deep alluvial deposits where basin-induced resonance is likely to occur

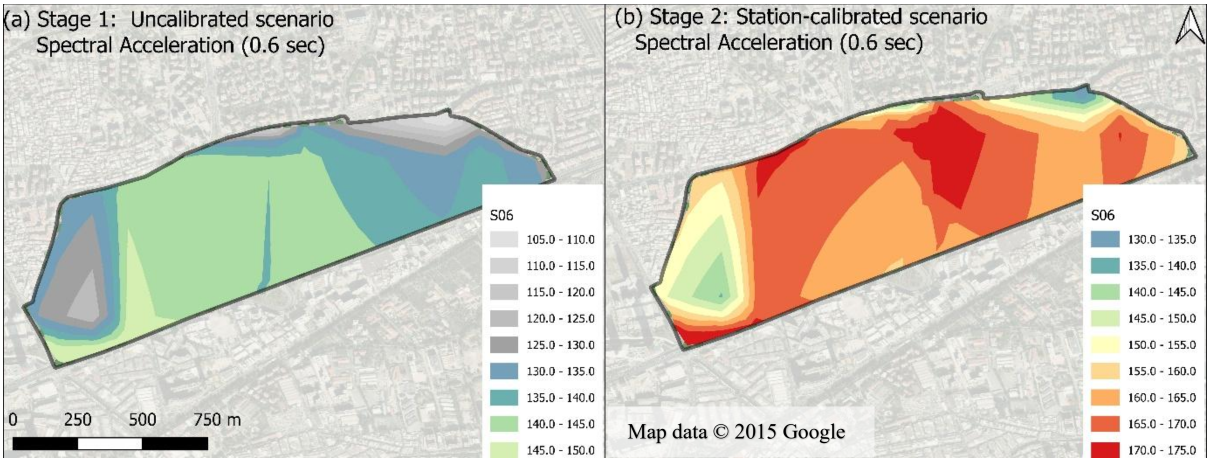

Figure 8. Comparison of Stage 1 (scenario-based) and Stage 2 (station-calibrated) Sa (T = 0.6 s) ShakeMaps for the Mansuroğlu Neighborhood. Base map source: © Google Maps 2015 (retrieved via QGIS QuickMapServices).

This period band (0.6 s- 1.0 s) is directly coupled with the fundamental vibration periods of the dominant building stock in the Mansuroğlu Neighborhood, which consists primarily of mid-to-high-rise reinforced concrete frame structures (typically 7–10 stories). Consequently, the underestimation of spectral demand in Stage 1 does not merely represent a modelling offset; it fails to capture the controlling factor in cumulative damage formation for the most vulnerable building typologies in the district. This discrepancy suggests that purely GMPEs-based ShakeMaps may lead to an 'optimistic bias' in damage forecasting, potentially delaying the mobilization of resources to areas where mid-rise structural failure is most probable.

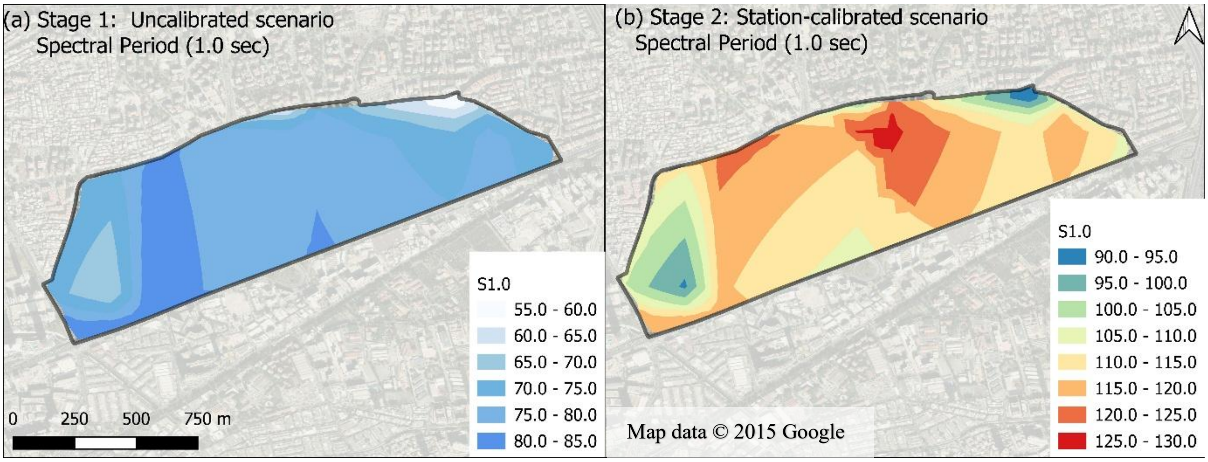

Figure 9. Comparison of Stage 1 (scenario-based) and Stage 2 (station-calibrated) Sa (T =1.0 s) ShakeMaps for the Mansuroğlu Neighborhood. Base map source: © Google Maps 2015 (retrieved via QGIS QuickMapServices).

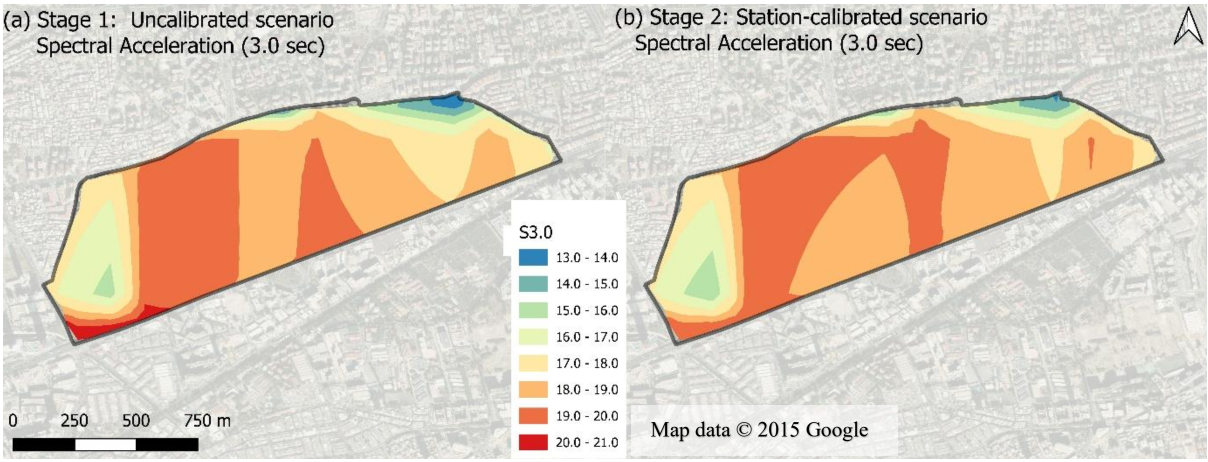

Figure 10. Comparison of Stage 1 (scenario-based) and Stage 2 (station-calibrated) Sa (T =3.0 s) ShakeMaps for the Mansuroğlu Neighborhood. Base map source: © Google Maps 2015 (retrieved via QGIS QuickMapServices).

The Sa (T=3.0 s) comparison (Figure 10) further highlights the limitations of purely scenario-based modelling in deep-basin settings. Whereas Stage 1 produces relatively smooth and spatially averaged long-period patterns, Stage 2 modifies both amplitude and spatial concentration, reflecting locally varying basin effects.

Overall, the incorporation of observational data does not merely adjust hazard magnitudes; it redistributes spectral demand spatially in a manner that is period-sensitive and structurally consequential. In a grid-based damage assessment framework, such redistribution may produce non-uniform shifts in cumulative damage exceedance probabilities across the study area. The implications of these exceedance shifts for operational response categorization are examined in the following section.

4.3. Cumulative Damage Assessment and Operational Implication

Cumulative damage and risk maps were derived for both the scenario-based (Stage 1) and station-calibrated (Stage 2) configurations using a grid-based framework. To enable consistent comparison with observed structural damage, a cumulative damage indicator {M+E+C} was defined by aggregating Moderate, Extensive, and Collapse damage states as shown in Fig. 11. This aggregation was adopted to represent buildings likely to require evacuation, structural inspection, or immediate intervention, thereby extending beyond isolated damage-class interpretation.

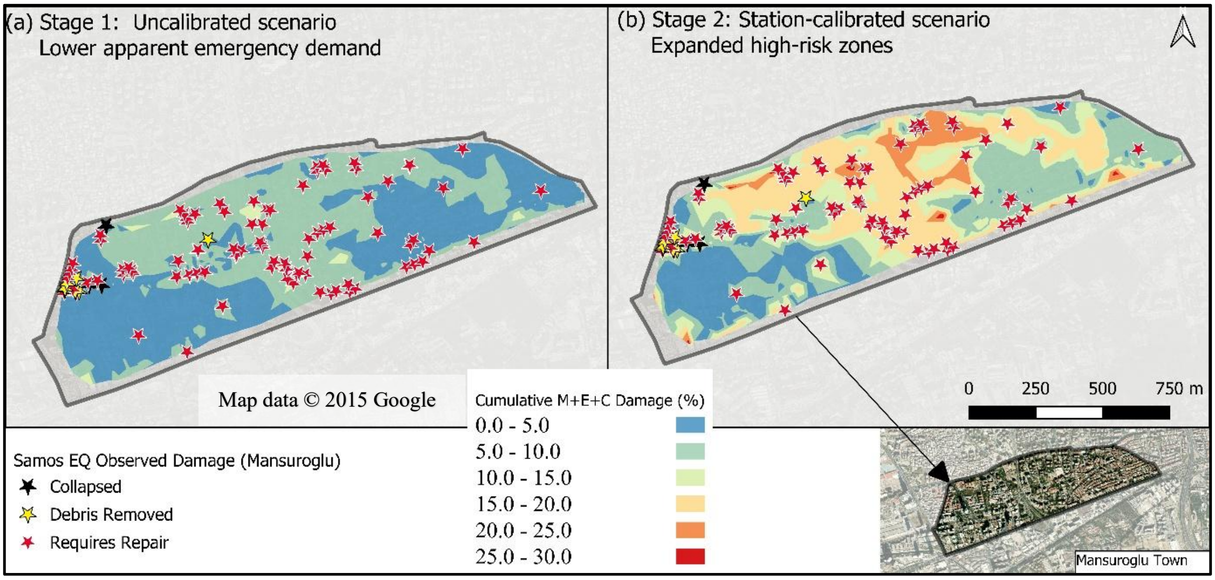

Figure 11. Cumulative damage probability maps {Moderate + Extensive + Collapse} derived from scenario-based (Stage 1) and station-calibrated (Stage 2) analyses. Base map source: © Google Maps 2015 (retrieved via QGIS QuickMapServices).

In operational terms, the {M+E+C} indicator functions not only as an engineering performance measure but also as a threshold-sensitive risk metric relevant to early-phase emergency response planning. Spatial distributions of this cumulative exceedance probability enable identification of districts where concentrated structural disruption may constrain accessibility and influence resource deployment strategies.

From an operational threshold perspective, station-based updating shifts the estimated cumulative damage exceedance probability {M+E+C} from the 5–10% range under the scenario-based configuration to approximately 15–30% following calibration. This shift represents a transition across an operationally meaningful exceedance level. In threshold-based response planning, such a transition may correspond to movement from a monitoring-oriented regime toward a mobilization-oriented regime, where debris management, corridor clearance, and intensified search-and-rescue deployment are prioritized. Given the time-critical nature of search-and-rescue operations (Coburn and Spence 2006; Yousefi et al. 2024), accurate delineation of these exceedance zones is essential for supporting timely and effective operational decision-making.

The divergence between scenario-based and station-updated exceedance probabilities highlights a governance-level sensitivity inherent in rapid model-driven assessments. When exceedance levels are underestimated, affected neighborhoods may appear comparatively less critical in the immediate aftermath of an event. Even moderate differences in exceedance estimation can influence prioritization decisions, inspection sequencing, and deployment intensity. In this context, misclassification emerges not as a purely statistical discrepancy, but as a decision-context issue arising from how ground-motion representations are translated into operational categories. In deep-basin environments, where intermediate-period amplification strongly governs structural response, such threshold-sensitive divergence becomes particularly consequential during the early response phase.

In densely built urban districts such as Mansuroğlu, cumulative damage exceedance levels approaching 15–30% may increase the likelihood of localized road obstruction due to debris accumulation, thereby challenging uniform accessibility assumptions embedded in emergency response planning. Under such conditions, response strategies may require area-specific prioritization. Zones characterized by relatively lower exceedance probabilities may function as potential medical access corridors, whereas zones with higher exceedance levels may be interpreted as mechanical intervention areas where debris removal resources and heavy equipment are allocated to restore accessibility and facilitate search-and-rescue operations.

Timely identification of these zones plays a central role in response effectiveness. A downward bias in exceedance estimation, often associated with purely scenario-based rapid assessments, may delay escalation of intervention intensity in severely affected districts. In time-critical response environments, even limited delays in recognizing high-obstruction zones may influence overall operational efficiency.

5 Conclusions

This study evaluated the ground-motion characteristics and observed damage distribution in the Mansuroğlu Neighborhood during the 30 October 2020 Samos earthquake within a two-stage operational framework: (i) a scenario-based rapid damage estimation (Stage 1) and (ii) a station-updated near-real-time configuration (Stage 2). By integrating strong-motion records from four AFAD stations located within a 3.0 km radius of the study area, the analysis explicitly quantified how observational updating modifies ground-motion representation and propagates into cumulative damage exceedance estimates that are directly relevant to early-phase emergency response.

From a ground-motion perspective, the scenario-based configuration (Stage 1) was found to systematically underrepresent seismic demand, particularly within the intermediate-period range (T = 0.6–1.0 s). While short-period demand exhibited only moderate variation, intermediate-period spectral accelerations increased markedly following station-based updating. This period band is critical for the Mansuroğlu Neighborhood, where the building stock is dominated by mid-rise reinforced concrete frame structures whose dynamic characteristics fall within this range. The enhanced spectral amplification captured in Stage 2 reflects resonance-related seismic demands that are not fully represented by purely GMPE-based scenario models in deep-basin environments. Consequently, the uncalibrated approach yields an overly optimistic representation of local seismic demand when compared with recorded observations and observed structural performance.

These differences propagate directly into cumulative damage exceedance estimates. Under the scenario-based configuration, the aggregated {Moderate + Extensive + Collapse} exceedance probability largely remains within the 0–10% range. In contrast, station-based updating increases this range to approximately 15–30%, aligning more closely with the observed spatial concentration of heavily damaged and collapsed buildings. This shift is not merely quantitative; it represents a transition across an operationally meaningful threshold. In a response-planning context, movement from a lower exceedance regime to a higher one may correspond to escalation from monitoring-oriented actions toward mobilization-oriented intervention, including intensified search-and-rescue deployment, debris management, and corridor clearance prioritization.

Accordingly, the findings demonstrate that operational damage misclassification may arise when scenario-based ShakeMaps underestimate exceedance probabilities associated with threshold-sensitive damage states. In deep-basin urban environments, where intermediate-period amplification governs structural response, such representational bias can translate into governance-level consequences during the golden hours of emergency management. Misclassification, in this context, is not solely a statistical modelling discrepancy but a decision-context distortion induced by ground-motion representation. Although the analysis focuses on the Izmir Bay basin, similar misclassification mechanisms may occur in other deep-basin urban environments where local amplification strongly influences intermediate-period spectral demand.

Despite the robustness of the two-stage framework, several limitations should be acknowledged. The station-updated configuration relies on a limited number of spatially proximate strong-motion stations (n = 4). Although the stations are spatially proximal to the study area, the availability of a denser strong-motion monitoring network would likely further refine bias correction and the spatial redistribution of spectral demand. The fragility assessment is based on HAZUS-derived vulnerability functions, which may not fully capture region-specific construction detailing and performance characteristics. In addition, construction year information was unavailable for a substantial portion of the building inventory, necessitating conservative assumptions regarding seismic design level. Finally, the analysis is based on a single earthquake case study within a deep-basin setting; therefore, extrapolation to other tectonic and urban contexts should be undertaken cautiously. Future research incorporating multi-event datasets and regionally calibrated fragility functions would further enhance the operational generalizability of the proposed framework.

Overall, this study demonstrates that operational damage misclassification extends beyond a technical modelling discrepancy and constitutes a risk management challenge with direct implications for time-critical emergency response during the ‘Golden Hours’. By shifting estimated damage exceedance from a monitoring-oriented to a mobilization-oriented regime, the results highlight the operational significance of incorporating observational data into near-real-time assessments. In this context, strong-motion monitoring networks emerge not merely as observational infrastructure, but as a fundamental component of operational seismic risk governance. Even a limited number of spatially proximate stations can substantially improve ShakeMap calibration and reduce uncertainty in exceedance-based damage estimation, thereby supporting more reliable and timely decision-making.

In this regard, the strategic densification and resilience of urban strong-motion networks should be considered a high-value investment for enhancing emergency response effectiveness and strengthening disaster risk management in basin-affected metropolitan regions.

Code, data, or code and data availability

Strong-motion records used in this study are available from the AFAD Strong Motion Database. Building inventory data were obtained from the Republic of Türkiye Ministry of Environment, Urbanization and Climate Change.

The analysis was conducted using the REDAS rapid damage estimation platform together with project-specific data processing workflows. The code used in this study is not publicly available.

Author contributions

F. İlknur Kara conceptualized the study, developed the methodology, performed the analyses, prepared the figures, and wrote the original manuscript.

Competing interests

The author declares that there is no conflict of interest.

Acknowledgements

The author would like to thank Prof. Yasin Fahjan for providing access to the REDAS platform and for valuable discussions. AI-based language assistance tools were used for language editing and clarity improvement. The scientific content, analysis, and conclusions are entirely the responsibility of the author.

Financial support

This research received no specific grant from any funding agency in the public, commercial, or not-for-profit sectors.

References

Abrahamson, N. A., Silva, W. J., and Kamai, R.: Summary of the ASK14 ground-motion relation for active crustal regions, *Earthquake Spectra*, 30, 1025–1055, https://doi.org/10.1193/070913EQS198M, 2014.

Askan, A., Gülerce, Z., Roumelioti, Z., Sotiriadis, D., Melis, N. S., Altindal, A., Akbaş, B., Sopaci, E., Karimzadeh, S., Kalogeras, I., Theodoulidis, N., Konstantinidou, K., Özacar, A. A., Kale, Ö., and Margaris, B.: The Samos Island (Aegean Sea) M7.0 earthquake: Analysis and engineering implications of strong-motion data, *Bulletin of Earthquake Engineering*, 20, 7737–7762, https://doi.org/10.1007/s10518-021-01251-5, 2021.

Boore, D. M., Stewart, J. P., Seyhan, E., and Atkinson, G. M.: NGA-West2 equations for predicting PGA, PGV, and 5 % damped PSA for shallow crustal earthquakes, *Earthquake Spectra*, 30, 1057–1085, https://doi.org/10.1193/070113EQS184M, 2014.

Bozorgnia, Y. et al.: NGA-West2 research project, *Earthquake Spectra*, 30, 973–987, https://doi.org/10.1193/072113EQS209M, 2014.

Campbell, K. W. and Bozorgnia, Y.: NGA-West2 ground-motion model for the average horizontal components of PGA, PGV, and 5 % damped linear acceleration response spectra, *Earthquake Spectra*, 30, 1087–1114, https://doi.org/10.1193/062913EQS175M, 2014.

Cetin, K. O. et al.: The site effects in Izmir Bay of October 30 2020 M7.0 Samos earthquake, *Soil Dynamics and Earthquake Engineering*, 152, 107051, https://doi.org/10.1016/j.soildyn.2021.107051, 2022.

Chiou, B. S. J. and Youngs, R. R.: Update of the Chiou and Youngs NGA model for the average horizontal component of peak ground motion and response spectra, *Earthquake Spectra*, 30, 1117–1153, https://doi.org/10.1193/072813EQS219M, 2014.

Coburn, A. and Spence, R.: *Earthquake Protection*, 2nd ed., Wiley, https://doi.org/10.1002/0470855185, 2006.

Day, S. M. et al.: Model for basin effects on long-period response spectra in Southern California, *Earthquake Spectra*, 24, 257–277, https://doi.org/10.1193/1.2857545, 2008.

Demirel, I. O., Yakut, A., and Binici, B.: Seismic performance of mid-rise reinforced concrete buildings in Izmir Bayraklı after the 2020 Samos earthquake, *Engineering Failure Analysis*, 137, 106277, https://doi.org/10.1016/j.engfailanal.2022.106277, 2022.

Disaster and Emergency Management Authority (AFAD): Preliminary damage and loss estimation system, available at: https://www.afad.gov.tr/on-hasar-ve-kayip-tahmin-sistemi, last access: 29 January 2026.

Dokuz Eylül University (DAUM): Samos earthquake report (30 October 2020), available at: https://daum.deu.edu.tr/wp-content/uploads/2020/11/Samos-Deprem-Raporu.pdf, last access: 24 January 2026 (in Turkish).

Erdik, M. et al.: Rapid earthquake loss assessment after damaging earthquakes, *Soil Dynamics and Earthquake Engineering*, 31, 247–266, https://doi.org/10.1016/j.soildyn.2010.03.009, 2011.

Federal Emergency Management Agency (FEMA): *Hazus Earthquake Model Technical Manual*, version 5.1, Washington, DC, 2022.

Federal Emergency Management Agency (FEMA): *Hazus Inventory Technical Manual*, version 6.1, Washington, DC, https://www.fema.gov, 2025.

Gülerce, Z. et al.: Predictive performance of current ground-motion models for recorded strong motions in the 2020 Samos earthquake, *Soil Dynamics and Earthquake Engineering*, 152, 107053, https://doi.org/10.1016/j.soildyn.2021.107053, 2022.

Hancilar, U. et al.: ELER software – a new tool for urban earthquake loss assessment, *Natural Hazards and Earth System Sciences*, 10, 2677–2696, https://doi.org/10.5194/nhess-10-2677-2010, 2010.

Izmir Metropolitan Municipality and Boğaziçi University: Izmir earthquake scenario and earthquake master plan, available at: https://izmir.bel.tr/izmirdeprem/, last access: 29 January 2026 (in Turkish).

Kiratzi, A. et al.: Characteristics of the 2020 Samos earthquake (Aegean Sea) using seismic data, *Bulletin of Earthquake Engineering*, 20, 7713–7735, https://doi.org/10.1007/s10518-021-01239-1, 2021.

Middle East Technical University (METU), EERC: Izmir earthquake report (30 October 2020), available at: https://eerc.metu.edu.tr/sites/eerc.metu.edu.tr/files/izmir_earthquake_report.pdf, last access: 24 January 2026.

Power, M. et al.: An overview of the NGA project, *Earthquake Spectra*, 24, 3–21, https://doi.org/10.1193/1.2894833, 2008.

QGIS.org (2024). QGIS Geographic Information System. QGIS Association. Version 3.42.2. https://www.qgis.org

RedACT project, available at: https://www.redact-project.eu/, last access: 8 November 2023.

SELENA-RISe Open Risk Package, available at: https://selena.sourceforge.net/selena.shtml, last access: 15 February 2026.

Silva, V. et al.: Development of the OpenQuake engine, *Natural Hazards*, 72, 1409–1427, https://doi.org/10.1007/s11069-013-0618-x, 2013.

Silva, V., Wald, D., and Taherian, A.: Potential benefits of seismic monitoring for ground-shaking estimation and loss assessment, *Bulletin of the Seismological Society of America*, 115, 1658–1676, https://doi.org/10.1785/0120240014, 2025.

United States Geological Survey (USGS): M 7.0 – 13 km NNE of Néon Karlovásion, Greece, available at: https://earthquake.usgs.gov/earthquakes/eventpage/us7000c7y0/executive, last access: 28 January 2026.

USGS Vs30 Map Viewer, available at: https://usgs.maps.arcgis.com/apps/webappviewer/index.html?id=8ac19bc334f747e486550f32837578e1, last access: 10 February 2026.

Yakut, A. et al.: Performance of structures in İzmir after the Samos Island earthquake, *Bulletin of Earthquake Engineering*, https://doi.org/10.1007/s10518-021-01226-6, 2021.

Yousefi, M. H. et al.: An auxiliary framework to facilitate earthquake search and rescue operations in urban regions, *Natural Hazards*, 120, 11107–11131, https://doi.org/10.1007/s11069-024-06619-9, 2024.

Zhao, D. et al.: A rapid estimation method for post-earthquake building losses, *International Journal of Disaster Risk Science*, 14, 428–439, https://doi.org/10.1007/s13753-023-00491-0, 2023.